ROZPRAWY INŻYNIERSKIE • ENGINEERING TRANSACTIONS • 22, 3, 487–508, 1974
Polska Akademia Nauk • Instytut Podstawowych Problemów Techniki

NUMERICAL SOLUTIONS OF THE VISCOUS FLOW PAST A CIRCULAR CYLINDER WITH STREAM-WISE VELOCITY FLUCTUATIONS

VINCENT P. GODDARD and ALBIN A. SZEWCZYK (NOTRE DAME)

Numerical solutions of the incompressible, two-dimensional, time-dependent Navier-Stokes equations have been obtained for the flow past a circular cylinder with free-stream velocity fluctuations in the flow direction. The fluctuations in the flow are produced by a change in magnitude only and not in direction. The resulting time-dependent equations are solved by the use of an explicit finite-difference scheme possessing conservative and transportive properties for a stream function-vorticity formulation. A variable mesh structure is selected to provide a cell size that is consistent with the structure of the flow, i.e., a fine mesh in regions of large gradients.

Results are presented for Reynold's number 40 and 200, and non-dimensionalized free-stream frequencies of 0.02 to 3.2. The results compare favorably with the analytical work of LIGHTHILL [9] and the experimental works of CHEN and BALLENGEE [2], and TATSUNO [16].

1. INTRODUCTION

This study deals with the numerical solutions of the homogeneous, incompressible, two-dimensional, time-dependent Navier-Stokes equations for the flow past a circular cylinder with free-stream velocity fluctuations. The fluctuations in the flow are produced by a change in magnitude only and not in direction.

From the inception of fluid mechanics, the analytical and experimental study of the flow past a circular cylinder has received more attention than any other flow problem, with the possible exception of that past a sphere. Although the geometry is simple, the flow phenomena especially in the wake are most complicated. The important basic nature of this problem and its importance as a keystone in fluid mechanics whether one considers real or ideal flow is well recognized. For example, potential flow studies with circulation about a circular cylinder have produced elegant explicit mathematical solutions for the lift. Then, through the utilization of conformal transformation techniques ideal-aerodynamic theory of airfoils was evolved. Such potential flow studies, however, provide no insight into the characteristics of the flow in the boundary layer, the drag, the formation of wakes and other realities of viscous flow. In order to account for these effects, one must consider the full Navier-Stokes equations with all of its non-linear complexities. The non-linearity of the equations poses formidable problems in obtaining satisfactory mathematical solutions. Hence, with the tremendous advance in high-speed computers and numerical techniques, a numerical approach is applied.

Various numerical solutions for the unsteady flow past a circular cylinder have appeared in the literature. For a complete listing see, e.g., THOMAN and SZEWCZYK

[17 and 18], ROACHE [12] and GODDARD [5]. The intent of this study was to extend numerical approach to the case, where the cylinder is immersed in an oscillating free stream. Such problems can arise when launch vehicles, smoke stacks and other circular structures, are subjected to unsteady winds. As a result unsteady forces are produced which give rise to undesirable motions of the vehicle or structure themselves.

LIGHTHILL [9] studied a similar flow situation where a flat plate oscillated parallel to a steady oncoming stream. In his study LIGHTHILL [9] also investigated analytically some aspects of the flow past a cylinder in a fluctuating stream. Experimentally only the works of CHEN and BALLENGEE [2] and most recently TATSUNO [16] on the vortex wakes behind a circular cylinder oscillating in the flow direction are presently known and have significant bearing on this study.

2. BASIC EQUATIONS

2.1. *Rectangular coordinates*

Consider the unsteady, two-dimensional, incompressible viscous flow past a circular cylinder of diameter D in an oscillating free stream. Using rectangular coordinates (x, y), the equations of motion in non-dimensional form can be written as

$$\frac{\partial \zeta}{\partial t}+\frac{\partial (u\zeta)}{\partial x}+\frac{\partial (v\zeta)}{\partial y}=\frac{1}{\mathrm{Re}}\left(\frac{\partial^2 \zeta}{\partial x^2}+\frac{\partial^2 \zeta}{\partial y^2}\right), \tag{2.1}$$

where $\mathrm{Re}=U_0 D/\nu$ is the Reynold's number, D being the characteristic length and ν the kinematic viscosity of the fluid. The stream function ψ, the vorticity ζ, and the velocity components (u, v) in the x and y directions, respectively, are specified by the following relations

$$\nabla^2 \psi=\frac{\partial^2 \psi}{\partial x^2}+\frac{\partial^2 \psi}{\partial y^2}=-\zeta, \tag{2.2}$$

$$u=\frac{\partial \psi}{\partial y}, \qquad v=-\frac{\partial \psi}{\partial x}. \tag{2.3}$$

2.2. *Polar coordinates*

A similar set of equations must be considered in polar coordinates (r, θ). The non-dimensional equations of motion can be written as

$$\frac{\partial \zeta}{\partial t}+\frac{1}{r}\left(\frac{\partial (rV_r \zeta)}{\partial r}+\frac{\partial (V_\theta \zeta)}{\partial \theta}\right)=\frac{1}{\mathrm{Re}}\left[\frac{1}{r}\frac{\partial}{\partial r}\left(r\frac{\partial \zeta}{\partial r}\right)+\frac{1}{r^2}\frac{\partial^2 \zeta}{\partial \theta^2}\right], \tag{2.4}$$

where

$$-\zeta=\frac{1}{r}\left[\frac{\partial}{\partial r}\left(r\frac{\partial \psi}{\partial r}\right)+\frac{1}{r}\frac{\partial^2 \psi}{\partial \theta^2}\right],$$

V_r and V_θ are components of velocity in the r and θ direction, respectively, given in terms of the stream function as $V_r=(1/r)\dfrac{\partial \psi}{\partial \theta}$ and $V_\theta=-\dfrac{\partial \psi}{\partial r}$.

3. Finite difference equations

The field of computation was defined on a grid system as shown in Fig. 1. This grid system divides the flow domain into two computational regions. The cylindrical region extends outward from the surface of the cylinder for a distance of one

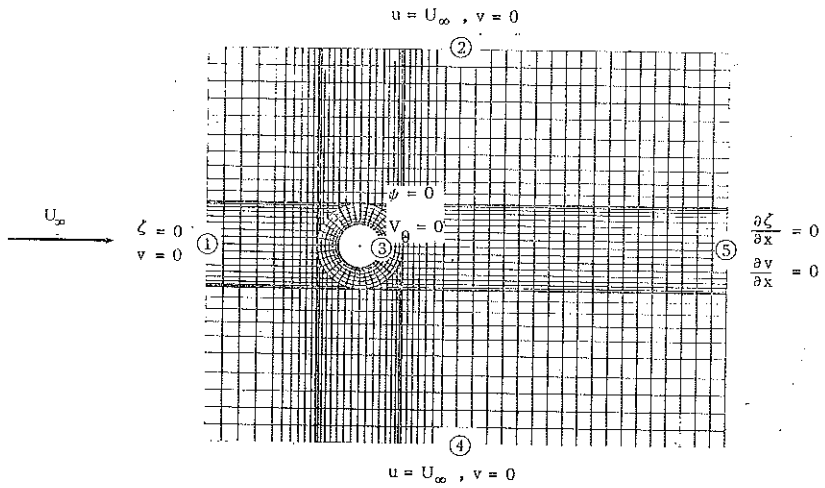

Fig. 1. Boundary conditions (stedy free stream)

radius. The cylindrical region is divided into cells of uniform arc divisions of 10 degrees. The radial divisions, 17 in all, are sized according to the Reynold's number being investigated. The remaining region is divided into a variable width rectangular cell structure.

3.1. Rectangular coordinates

The values of any function for a typical interior rectangular cell with its four adjacent cells is associated with the center of the cell and is denoted by the subscripts (i, j). The four surrounding cells are labeled with reference to the pivotal cell. The mid-points on the borders of the pivotal cell are referenced by half-subscripts. The variable rectangular cell widths and heights are designated by the notation B_i and A_j.

In order that the calculational stability of the voticity transport equation be augmented, use is made of a directional differencing scheme for the non-linear convective terms, e.g., see Thoman and Szewczyk [17 and 18] and Roache [12]. This scheme takes the values of vorticity at the mid-point of the cell's borders as being equal to those of the cells from which the vorticity is being convected. Using the ordinary forward differencing scheme for the time derivatives and the "directional

differencing" for the non-linear convective terms, the finite difference approximation of the non-dimensional vorticity transport equation is,

$$(3.1)\quad \frac{\zeta_{i,j}^{k+1}-\zeta_{ij}^{k}}{\Delta t}+\frac{(u\zeta)_{i+1/2,j}^{k}-(u\zeta)_{i-1/2,j}^{k}}{B_i}+\frac{(v\zeta)_{i,j+1/2}^{k}-(v\zeta)_{i,j-1/2}^{k}}{A_j}=$$

$$=\frac{1}{\mathrm{Re}}\left\{\frac{2}{\alpha_i(1+\alpha_i)\Delta x_i^2}[\alpha_i\zeta_{i-1,j}^{k}-(1+\alpha_i)\zeta_{i,j}^{k}+\zeta_{i+1,j}^{k}]+\right.$$

$$\left.+\frac{2}{\beta_j(1+\beta_j)\Delta y_j^2}[\beta_j\zeta_{i,j-1}^{k}-(1+\beta_j)\zeta_{i,j}^{k}+\zeta_{i,j-1}^{k}]\right\},$$

where $\alpha_i=(x_{i+1}-x_i)/(x_i-x_{i-1})$, $\beta_j=(y_{j+1}-y_j)/(y_j-y_{j-1})$ and the superscripts (k) and $(k+1)$ indicate current and advanced values of the function. Solving equation (2.2) in finite difference form for an explicit expression of $\psi_{i,j}$ yields,

$$(3.2)\quad \psi_{i,j}=RDXY_{i,j}[\zeta_{i,j}+APSI_i\,\psi_{i-1,j}+BPSI_i\,\psi_{i+1,j}+$$

$$+CPSI_j\,\psi_{i,j-1}+DPSI_j\,\psi_{i,j+1}],$$

where $RDXY_{i,j}=[2/\alpha_i\,\Delta x_i^2+2/\beta_j\,\Delta y_j^2]^{-1}$, $APSI_i=2\,[(1+\alpha_i)\,\Delta x_i^2]^{-1}$, $BPSI_i=2\,[\alpha_i(1+\alpha_i)\,\Delta x_i^2]^{-1}$, $CPSI_j=2\,[(1+\beta_j)\,\Delta y_j^2]^{-1}$, and $DPSI_j=2\,[\beta_j(1+\beta_j)\,\Delta y_j^2]^{-1}$.

The non-dimensional velocities and stream-function take on the following finite difference form:

$$(3.3)\quad u_{i,j}=-AU_j\,\psi_{i,j-1}-BU_j\,\psi_{i,j}+CU_j\,\psi_{i,j+1},$$

$$(3.4)\quad v_{i,j}=AV_i\,\psi_{i-1,j}+BV_i\,\psi_{i,j}+CV_i\,\psi_{i+1,j},$$

where

$$AU_j=\beta_j^2\,[\beta_j(1+\beta_j)\,\Delta y_j]^{-1},\quad BU_j=(1-\beta_j^2)\,[\beta_j(1+\beta_j)\,\Delta y_j]^{-1},$$

$$CU_j=[\beta_j(1+\beta_j)\,\Delta y_j]^{-1},\quad AV_i=\alpha_i^2\,[\alpha_i(1+\alpha_i)\,\Delta x_i]^{-1},$$

$$BV_i=(1-\alpha_i)^2\,[\alpha_i(1+\alpha_i)\,\Delta x_i]^{-1},\quad CV_i=[\alpha_i(1+\alpha_i)\,\Delta x_i]^{-1}.$$

3.2. Polar coordinates

The values of any function for a typical interior cylindrical cell with its four adjacent cells is associated with the center of the cell and is denoted by the subscripts $(ir, i\theta)$. Similar to the rectangular system, the mid—points of the cells borders are referred to by half subscripts. The variable cell radial length is denoted by DR_{ir} and the uniform angular division by $\Delta\theta$.

The finite difference representation of the polar transport equation takes the form

$$(3.5)\quad \frac{\zeta_{ir,i\theta}^{k+1}-\zeta_{ir,i\theta}^{k}}{\Delta t}+\frac{(rV_r\,\zeta)_{ir+1/2,i\theta}^{k}-(rV_r\,\zeta)_{ir-1/2,i\theta}^{k}}{r_{ir}\,DR_{ir}}+$$

$$+\frac{(V_\theta\,\zeta)_{ir,i\theta+1/2}^{k}-(V_\theta\,\zeta)_{ir,i\theta-1/2}^{k}}{r_{ir}\,\Delta\theta}=$$

(3.5) [c.d.]
$$= \frac{1}{\mathrm{Re}} \left\{ \left[\frac{2}{(1+\lambda_{ir})\,\Delta r_{ir}^2} - \frac{1}{(1+\lambda_{ir})\,r_{ir}\,\Delta r_{ir}^2} \right] \zeta_{ir-1,i\theta} + \right.$$
$$+ \left[\frac{2}{\lambda_{ir}(1+\lambda_{ir})\,\Delta r_{ir}^2} + \frac{1}{\lambda_{ir}(1+\lambda_{ir})\,r_{ir}\,\Delta r_{ir}^2} \right] \zeta_{ir+1,i\theta} + \frac{1}{r_{ir}^2\,\Delta\theta^2}\,[\zeta_{ir,\theta-1} + \zeta_{ir,\theta+1}] -$$
$$\left. - \left[\frac{1}{\frac{2(1+\lambda_{ir})}{\lambda_{ir}(1+\lambda_{ir})\,\Delta r_{ir}^2} + \frac{(1-\lambda_{ir}^2)}{\lambda_{ir}(1+\lambda_{ir})\,r_{ir}\,\Delta r_{ir}} + \frac{2}{r_{ir}^2\,\Delta\theta^2}} \right] \zeta_{ir+1,i\theta} \right\},$$

where $\lambda_{ir} = (r_{ir+1} - r_{ir})/(r_{ir} - r_{ir-1})$.

The explicit expression for $\psi_{ir,i\theta}$ takes the form,

(3.6)
$$\psi_{ir,i\theta} = RDRT_{ir}\,\{\zeta_{ir,i\theta} + APSIC_{ir}\,\psi_{ir-1,i\theta} + BPSIC_{ir}\,\psi_{ir+1,i\theta} + CPSIC_{ir}\,[\psi_{ir,i\theta-1} + \psi_{ir,i\theta+1}]\}$$

where

$$RDRT_{ir} = \left[\frac{2}{\Delta r_{ir}^2\,\lambda_{ir}} + \frac{(1-\lambda_{ir})}{\lambda_{ir}\,r_{ir}\,\Delta r_{ir}} + \frac{2}{r_{ir}^2\,\Delta\theta^2} \right]^{-1},$$

$$APSIC_{ir} = \frac{2}{(1+\lambda_{ir})\,\Delta r_{ir}^2} - \frac{\lambda_{ir}}{(1+\lambda_{ir})\,r_{ir}\,\Delta r_{ir}},$$

$$BPSIC_{ir} = \frac{2}{\lambda_{ir}(1+\lambda_{ir})\,\Delta r_{ir}^2} + \frac{1}{\lambda_{ir}(1+\lambda_{ir})\,r_{ir}\,\Delta r_{ir}},$$

$$CPSIC_{ir} = \frac{1}{r_{ir}^2\,\Delta\theta^2}.$$

The radial and tangential non-dimensional finite difference expressions for the velocities are

(3.7)
$$V_{r_{ir,i\theta}} = AVR_{ir}\,[\psi_{ir,i\theta-1} - \psi_{ir,i\theta+1}],$$

(3.8)
$$V\theta_{ir,i\theta} = AVT_{ir}\,\psi_{ir-1,i\theta} + BVT_{ir}\,\psi_{ir,i\theta} - CVT_{ir}\,\psi_{ir+1,i\theta}.$$

where

$$AVT_{ir} = [2r_{ir}\,\Delta\theta]^{-1},\quad AVT_{ir} = \lambda_{ir}^2\,[\lambda_{ir}(1+\lambda_{ir})\,\Delta r_{ir}]^{-1},$$

$$BVT_{ir} = (1-\lambda_{ir}^2)\,[\lambda_{ir}(1+\lambda_{ir})\,\Delta r_{ir}]^{-1},\quad \text{and}\quad CVT_{ir} = [\lambda_{ir}(1+\lambda_{ir})\,\Delta r_{ir}]^{-1}.$$

3.3. Initial and boundary conditions

a. Steady freestream. In seeking the solution of the time dependent problem an initial solution must be specified at time $t=0$, and boundary conditions on all boundaries for all subsequent times. Care must be exercised in specifying not only the initial solution but the boundary conditions as well, so that the end solution will correspond in actuality to the desired one.

The initial solution for the non-dimensional stream function of the flow past a circular cylinder is as follows:

(3.9) rectangular region: $$\psi_{i,j}=y_j\left[1-\frac{0.25}{x_i^2+y_j^2}\right],$$

(3.10) cylindrical region: $$\psi_{ir,i\theta}=\left[1-\frac{0.25}{r_{ir}^2}\right]r_{ir}\sin\theta_{i\theta}.$$

The boundary conditions are shown in Fig. 1. On the inflow boundary, the conditions of zero vorticity and zero v-velocity are specified, whereas on the outflow boundary the conditions that the change in the v-velocity and the vorticity in the downstream direction is zero are specified. These conditions have been successfully applied before by THOMAN and SZEWCZYK [17 and 18] and have been used by other investigators since, see ROACHE [12].

On the upper and lower boundary the flow is considered uniform and parallel. In effect, it is assumed that these boundaries are remote enough that the flow can be treated as parallel, so that the conditions correspond to a frictionless (or moving) wind tunnel wall.

On the cylinder surface the stream function is specified to be a constant (zero). In addition the condition of no slip on a stationary solid surface requires that the radial and tangential velocities be set equal to zero.

b. Fluctuating freestream. The initial condition or solution for a given Reynolds number flow for the fluctuating freestream problem was either the steady state or the limit cycle solution of the steady freestream problem. The inflow, outflow and cylinder surface boundary conditions for an oscillating freestream were identical to those used for the steady freestream problem. Since the magnitude of the oncoming velocity and not its direction is permitted to vary, the conditions imposed on the velocities at these boundaries were

(3.11) $$u=U_\infty=\bar{U}_\infty\,(1+\mathbf{Amp}\sin\omega t),$$
$$v=0,$$

where $\bar{U}_\infty$ is the steady mean freestream velocity about which the oscillations occur. **Amp** is the velocity amplitude and ω is the circular frequency.

3.4. Numerical stability

Numerical stability is one of the major factors that influences the choice of a finite difference scheme. For a detailed description and development of the stability criterion used in this study, see the works of GODDARD [5], ROACHE [12] and THOMAN and SZEWCZYK [17 and 18]. The von Neuman stability criteria require

(3.12) $$\Delta t_{\text{diffusion}}\leqslant \mathrm{Re}\cdot RDXY_{i,j},$$

and

(3.13) $$\Delta t_{\text{convective}}\leqslant\left[\frac{|u_{i,j}|}{B_i}+\frac{|v_{i,j}|}{A_j}\right]^{-1}.$$

Since both criteria must be met simultaneously, we have

$$\Delta t_{\text{critical}} \leqslant \left[\frac{1}{\Delta t_{\text{diffusion}}} + \frac{1}{\Delta t_{\text{convective}}} \right]^{-1}. \tag{3.14}$$

A similar analysis can be applied to the cylindrical form of the equations. The resulting expressions are

$$\Delta t_{\text{diffusion}} \leqslant \text{Re} \cdot RDRT_{ir}, \tag{3.15}$$

and

$$\Delta t_{\text{convective}} \leqslant \left[\frac{|Vr_{ir,i\theta}|}{Dr_{ir}} + \frac{|V\theta_{ir,i\theta}|}{r_{ir}\,\Delta\theta} \right]^{-1}. \tag{3.16}$$

Since $\Delta t_{\text{critical}}$ varies from cell to cell a search of the entire flow field must be made to determine the allowable critical time step. The value of the time step used for a given calculation was determined from $\Delta t = \eta \Delta t_{\text{critical}}$ where $0.3 \leqslant \eta \leqslant 0.9$. In general, a small time step required a fewer number r of iterations to satisfy Poisson's equation for the streamfunction.

3.5. Convergence

The solution of Poisson's equation for the streamfunction is obtained iteratively. In the solution of this equation the criterion requires that $|\psi^{n+1}_{i,j} - \psi^{n}_{i,j}|_{\max} < \varepsilon$ when n is the number of iterations and ε is some small pre-assigned value. The value can be determined by numerical experimentation. The value used for most cases in this investigation was 1×10^{-4}.

When a steady flow solution is expected as a result, a criterion similar to that given above can be formulated. The steady flow solution will be approached asymptotically, so in place of the iteration index n, we use the time step k. The convergence criterion for the vorticity is $|\zeta^{k+1}_{i,j} - \zeta^{k}_{i,j}| < \gamma$, where γ is some small pre-assigned value.

In addition to convergence, for the unsteady flow past a cylinder where vortex shedding occurs, one must ascertain when a limit cycle has been reached. In practice for both the steady and unsteady flow cases, comparison of the computer solution with experimental data and/or known analytical solutions provides a reasonable indication of a correctly converged solution.

4. Pressure, drag and lift coefficients

The pressure distribution on the cylinder itself is obtained directly from the momentum equations. The pressure terms in the momentum equation for the rectangular coordinate system can be expressed as

$$\frac{\partial p}{\partial x} = \frac{1}{2} \rho \frac{U_\infty^2}{D} \frac{\partial C_p}{\partial x}, \tag{4.1}$$

and

$$\frac{\partial p}{\partial y}=\frac{1}{2}\rho\frac{U_\infty^2}{D}\frac{\partial C_p}{\partial y}, \tag{4.2}$$

where $C_p=(p-p_\infty)\Big/\frac{1}{2}\rho U_\infty^2$. Similar equations govern the pressure coefficient in the polar coordinate system. Integration of equations (4.1) and (4.2) are performed numerically to obtain the pressure distribution on the cylinder.

From the pressure distribution and vorticity distribution on the cylinder the total drag coefficient due to pressure and friction is $C_D=C_{DP}+C_{DF}$ giving

$$C_D=-\int_0^{2\pi} C_P\cos\theta\,d\theta-\frac{1}{\mathrm{Re}}\int_0^{2\pi}\zeta\sin\theta\,d\theta. \tag{4.3}$$

In a similar way the lift coefficient is expressed as $C_L=C_{LP}+C_{LF}$ giving

$$C_L=\int_0^{2\pi} C_P\sin\theta\,d\theta+\frac{1}{\mathrm{Re}}\int_0^{2\pi}\zeta\cos\theta\,d\theta. \tag{4.4}$$

5. Computatiom procedure

Only an outline of the numerical procedure is given here. For details the reader is referred to Goddard [5].

The initial calculations begin with computation of the mesh system and the necessary constants for the streamfunction and vorticity transport equations. Next, the initial potential flow solution was computed and then modified to conform to the boundary conditions by an iterative scheme. After convergence the velocity and cylinder surface vorticity were computed. With the problem totally initialized, the time is advanced and the following repetitive calculational procedure is applied:

1. At the beginning of a time step all required quantities for each mesh point are known.
2. For each cell center an advanced value of ζ is calculated.
3. Knowing ζ current values of ψ's are computed.
4. From ψ's current velocities are computed and the surface vorticity updated.
5. At selected time levels, the pressure distribution, lift and drag are determined and a summary print-out is made.
6. The steps 1 through 5 are repeated until desired temporal state is reached.

6. Results: analysis and discussion

Solutions for the flow past a circular cylinder started impulsively from rest in a fluctuating free-stream for Reynold's numbers 40 and 200 are presented in detail. In addition some of the results obtained for a steady freestream at the same Reynold's numbers are presented to establish the validity of the basic time-dependent formulation and numerical scheme.

6.1. *Steady free-stream solutions*

Steady state solutions for the flow at Reynold's numbers 40 and 200 provided stream function and vorticity contours. For a Reynold's number of 40, the steady state solution shows that the flow is symmetrical about the x-axis and that a symmetrical vortex pair is formed in the wake and remains attached to the rear of the cylinder. For details see GODDARD [5]. The length of the standing vortices compares favorably with other numerical results e.g., THOMAN and SZEWCZYK [17 and 18] and TAKAMI and KELLER [14]. It is well known that wind tunnel walls have a strong effect upon the wake and its development and to a much lesser degree an influence upon other flow regions. In this study the upper and lower boundary conditions used correspond, in effect, to frictionless tunnel walls with a cylinder diameter to tunnel height ratio, $D/h=0.1$. With these constraints in mind the results obtained are compared with the experimental results of TANEDA [15] and GROVE *et. al.* [6] in Fig. 2.

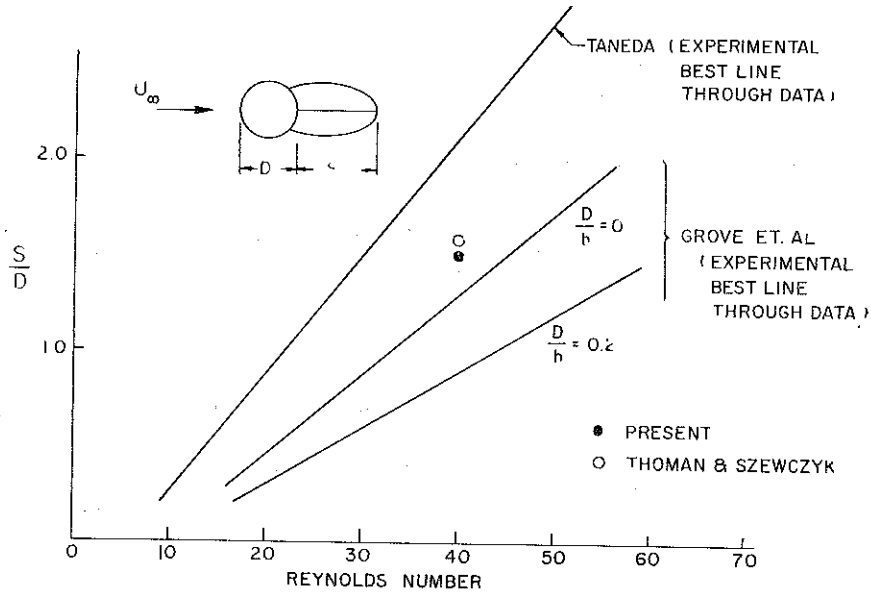

FIG. 2. Length of standing vortices, steady free-stream

For a Reynold's number of 200, the flow is not symmetrical with time and the formation of a vortex street is observed in contrast to the symmetrical vortex pair obtained for Reynold's number 40. These flow patterns are in good agreement with visual flow experiments at similar Reynold's numbers.

The variation of the separation angle with Reynold's number, the variation of the drag coefficient with Reynold's number, and the pressure coefficient for Reynold's number of 40 is shown in Figs. 3, 4, and 5, respectively. Good agreement is found for the results of the present study and data from other numerical studies and experimental observations.

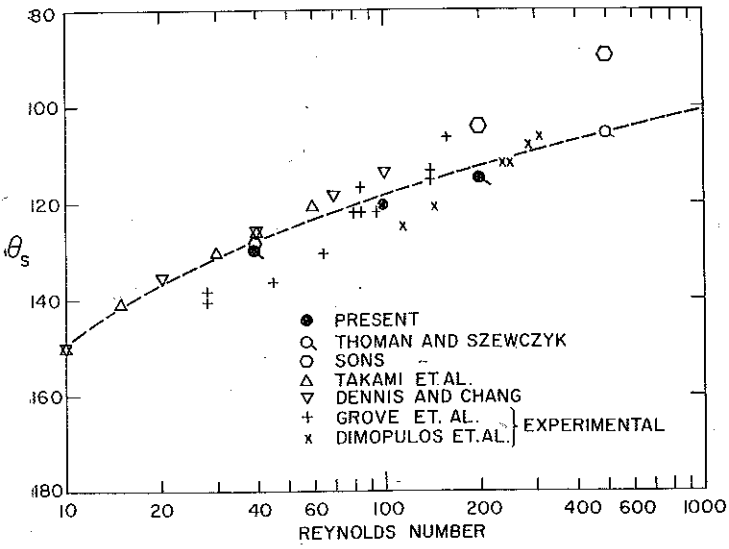

FIG. 3. Separation angle vs Reynolds number, steady free-stream

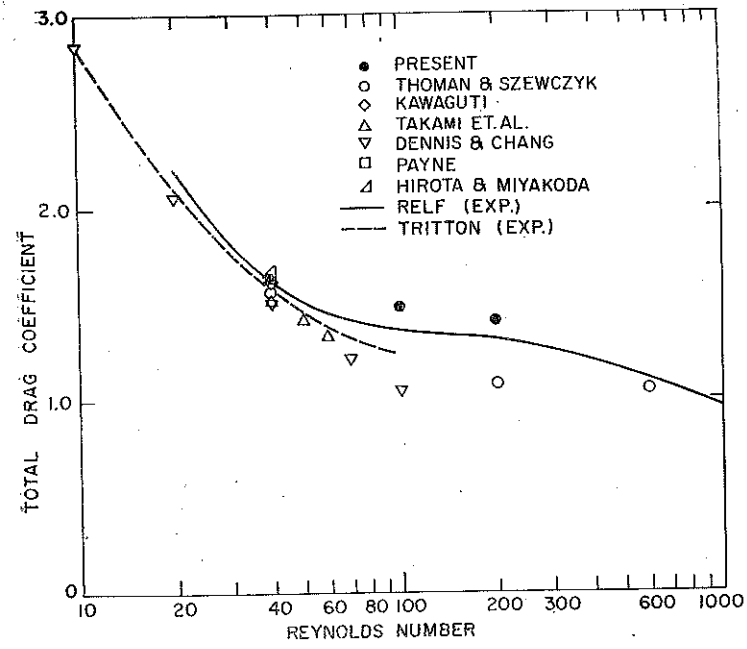

FIG. 4. Drag coefficient vs Reynolds number, steady free-stream

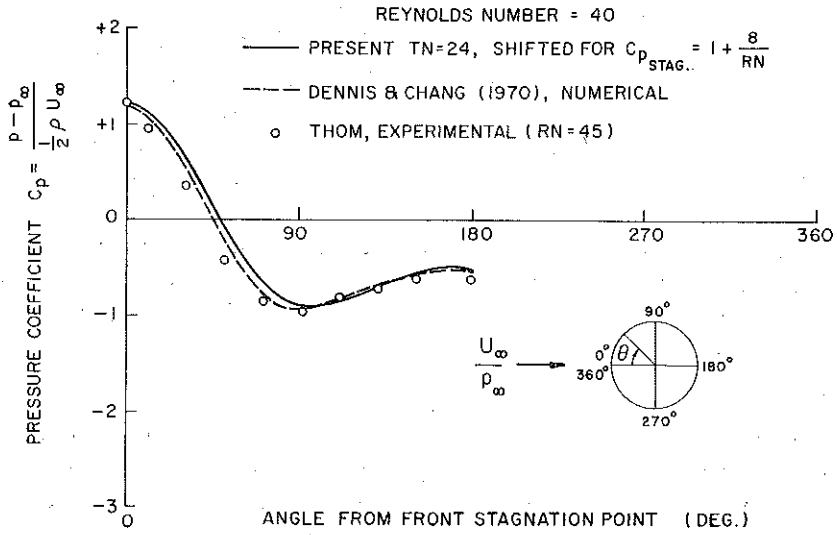

FIG. 5. Pressure coefficient collate experimental, steady free-stream

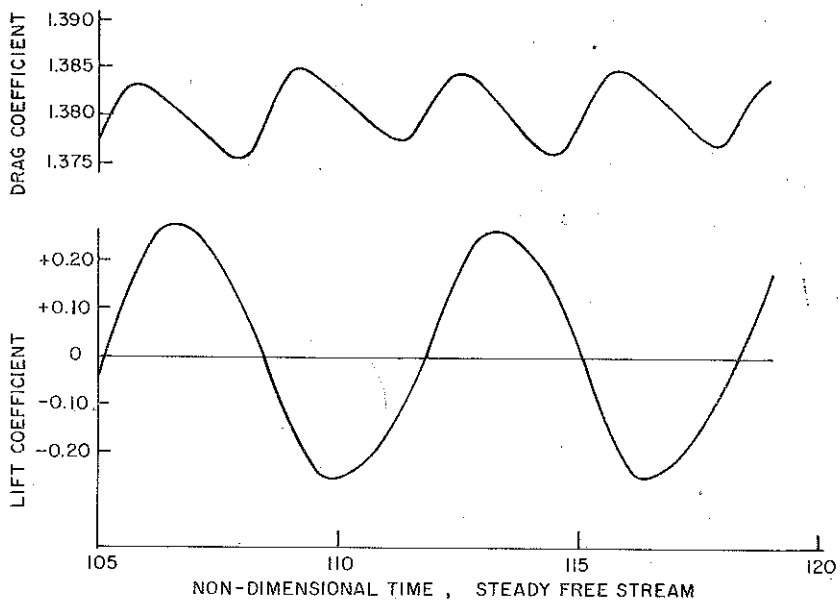

FIG. 6. Drag and lift vs time, steady free-stream Re=200

At a Reynold's number of 200 the vortices formed at the rear of the cylinder are shed alternately and form the well known Kármán vortex street. The frequency of shedding was evaluated from the cyclic lift curves and was determined to be 0.149. The fluctuating lift is shown in Fig. 6. In addition to the total mean drag due to the pressure and friction drag, and the fluctuating lift, the fluctuating drag acting on the cylinder is discernable. Although the fluctuating drag force is very small compared with the lift and mean drag forces, as observed by BISHOP and HASSAN [1], Fig. 6 shows the magnitude and frequency of this force. A further comparison of the frequencies of the fluctuating lift and drag coefficients shows that the fluctuating drag has a frequency of twice that of the lift as expected. Very little experimental data is available for direct comparison at this Reynolds number because of the difficulty in detection of these forces in experimental investigations.

6.2. Fluctuating free-stream

Steady and fluctuating free-stream results and salient characteristics are presented in Table 1. For the fluctuating freestream, Reynold's numbers of 40 and 200 were investigated. Low, medium and high frequency free-stream oscillations corresponding to freestream Strouhal numbers of 0.019, 0.120 and 3.180, respectively, were

Table 1. Summary of computer runs

Reynolds number	40			200	
Free-stream	Steady	Fluctuating		Steday	Fluctuating
ω_N	—	0.12	0.75	20.0	—	0.935
Free stream Fluctuation freq.	—	0.019	0.12	3.18	wake freq. =0.149	0.149
Fluctuation Amp.	—	0.20	0.10	0.10	—	0.10
Computed time advance for						
$C_{D\ total}$	—	essentially none	0.50	0.05	—	0.90
$C_{D\ friction}$	—	essentially none	0.40	0.025	—	0.50
Cycles computed	—	one	four	five	limit cycle at time=59	
Time	33.5	24.0—81.0	24.0—58.0	23.9—25.5	70.0	64.0=89.0

investigated at a Reynold's number of 40. For a Reynold's number of 200, only that frequency corresponding to the natural frequency in steady flow, St=0.149, was investigated. All of the cases investigated were initiated by an impulsive start from the steady state solution corresponding to a non-dimensional time of 23.9.

a. Ryenold's number 40. i. *Low frequency* — St=0.019. This is an extremely slowly varying free-stream oscillation. The effect of the impulsive start is quite apparent at the very beginning but is quickly damped out. The velocity reached its first maximum at a non-dimensional time of 37.0. No apparent lead or lag in the friction drag of the cylinder was discernable at this time. It was found that the peak in the friction drag coefficient was in near alignment with the velocity maximum. The pressure component of the drag coefficient and, so consequently, the total drag coefficient did not follow the free-stream variations nearly as well. Furthermore, the pressure drag lagged slightly behind the free-stream velocity by nearly one non-dimensional time unit.

In comparing these results with the experimental results of Chen and BALLENGEE [2] it can be concluded that for a slowly varying free-stream velocity the drag of the cylinder responds instantaneously and is equal to the steady state value associated with the instantaneous value of the velocity. Thus the instantaneous drag coefficient is given by the ratio of the change in dynamic pressure, namely

$$C_{D\,\text{instant}} = C_{D\,\text{steady}} \left(\frac{U_\infty}{\bar{U}_\infty} \right)^2 . \tag{6.1}$$

LIGHTHILL predicted that the local skin friction would anticipate the free-stream fluctuations. Results for this case show that the vorticity maximums lag the velocity maximums at 25° and 45°. These points are in the region where Lighthill's analysis is valid and the vorticity maximums should have anticipated the velocity maximums by a non-dimensional time of 0.05 corresponding to a phase angle $\Phi = 20.4$ minutes. At 105° and 115° in the region just prior to separation where Lighthill's "stagnation region" solution is not considered applicable, the vorticity maximum does lead the velocity maximum. Furthermore, Lighthill speculates that the separation point would fluctuate, however for this Reynold's number and frequency, fluctuation of the separation point was not discernable. From the instantaneous streamline patterns for the flow around the cylinder at various times throughout a cycle of velocity fluctuations, it was found that the length of the standing vortices change throughout the cycle and that the maximum length appears at the minimum drag point. Correlation between the length of the standing vortices at the extreme drag points is explained in the following section.

ii. *Medium frequency* — St=0.12. The medium non-dimensional, free-stream velocity fluctuation of St=0.12 was chosen since it was estimated to be the value that would approximate the natural shedding frequency of a cylinder at a Reynold's number of 40 if the cylinder could be forced to shed by some anomalous disturbance. It was tacitly assumed that if the streamwise velocity fluctuations could induce an alternate vortex shedding pattern it would in some likelihood occur at this frequency. No vortex shedding was found to occur at this Reynold's number, however a growth and decay of the attached wake vortex bubble was observed as shown in Figs. 9 and 10.

Figure 7 shows the computed response of the total drag coefficient, together with its components due to pressure and friction, to the fluctuations in streamwise

velocity. The effect of the impulsive start is not very apparent at this frequency and its effect is observable only for times somewhat less than 1/4 of the first cycle. In order to be assured of stable and repetitive results, the computer solutions were extended for a total of four complete cycles. Inspection of Fig. 7 indicates that the cyclic variations of the drag coefficients are exactly the same after the first cycle where the effects of the impulsive start occur.

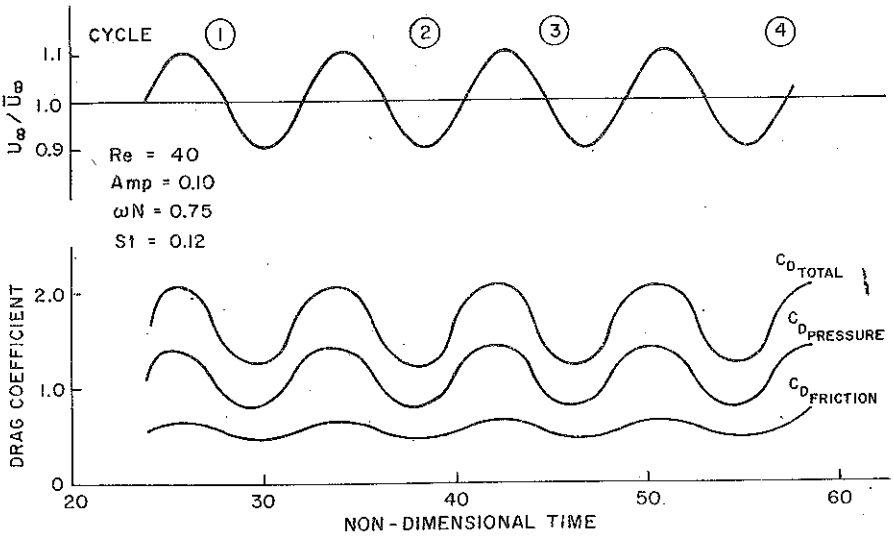

FIG. 7. Drag response to free-stream fluctuations Re=40, St=0.12

It is seen in Fig. 7 that the total pressure and friction drag do anticipate the velocity extrema. The pressure drag lead is greater than that of the friction drag and since the total drag is their sum, the total drag lead lies between the two.

In Fig. 8 the computed response of the vorticity on the cylinder surface corresponding to angles measured from the front stagnation point of 15°, 25°, 45°, 105° and 115° is presented. The cyclic variation is presented only for the third and fourth cycles where the effects of the impulsive start have vanished. For this frequency, Lighthill's analysis predicts a phase advance of two degrees and nine minutes corresponding to a time advance of 0.05. In the front quadrant it is with uncertainty that any visible phase change can be seen other than a slight lag. This lag is more noticeable at the smaller angles. At angles nearer to separation, i.e., 105° and 115° the phase advance is quite definite and approaches that predicted by Lighthill's shear-flow model. It is of interest at this point to note that within the plotting accuracy of Fig. 7 the total friction drag coefficient for the cylinder does show a phase advance, as was previously noted, and that the corresponding time advance is equal to 0.40 non-dimensional time units.

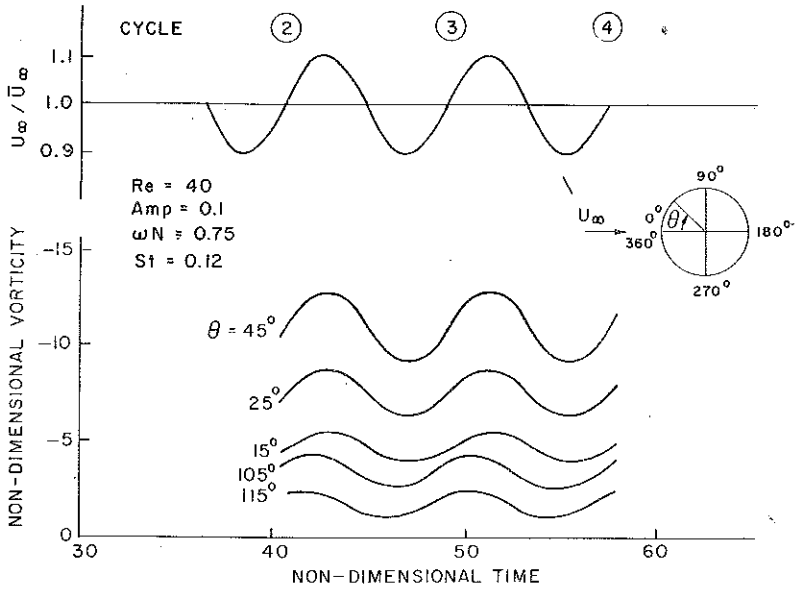

FIG. 8. Vorticity response to free-stream fluctuations Re=40, St=0.12

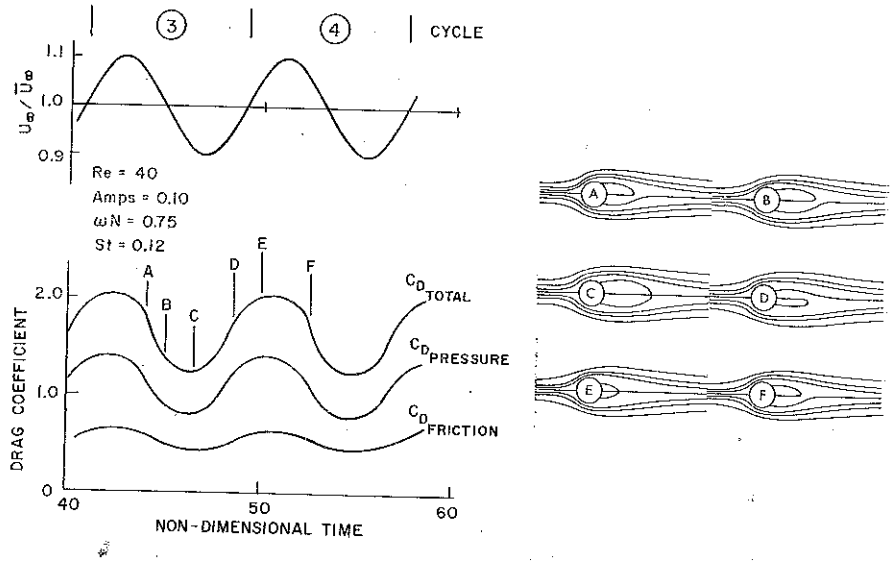

FIG. 9. Flow patterns, fluctuating free-stream Re=40, St=0.12

The instantaneous streamline patterns that exist at various points during the third and fourth cycle are shown in Fig. 9. Similar to the low frequency case the length of the standing vortices increases with decreasing velocity. The maximum length corresponds to the minimum drag point and the minimum length to the maximum drag point. The relationship between the length of the standing vortices and the drag coefficient is in accord with the physical situation. That this is so can be deduced from the steady flow results. Figure 3 shows that the length of standing vortices increases with Reynold's number, while Fig. 4 shows that the drag coefficient decreases with Reynold's number. Thus the drag coefficient varies inversely with the length of the standing vortices.

Lastly, these flow patterns indicate that the separation point fluctuates with the fluctuating freestream velocity. This is in accord with Lighthill's prediction.

iii. *High frequency* — St=3.18. This value of the non-dimensional frequency of fluctuation of the free-stream velocity was selected because it corresponds to the critical frequency. The critical frequency is that frequency at the boundary between the low and high frequency expansion methods used by Lighthill in his analysis, where the results from both methods are identical. When the frequency is equal to or greater than the critical, the phase advance angle of the skin friction is 45 degrees.

The effects from the impulsive start were quite apparent in this case during the first two or three cycles and only the fourth and fifth cycles provided results that were repetitive. Here as in the previous two cases the friction drag coefficient variation is quite smooth and sinuous with a phase advance. This was also true of the pressure and total drag coefficients. The friction drag coefficient of the cylinder anticipates the velocity extrema by about 0.025 time units, whereas the total drag coefficient anticipates the velocity extrema by nearly twice this amount. That the drag coefficients anticipate the velocity extrema, without exception, is noteworthy. For this frequency a very definite phase advance for the surface vorticity is found over the whole cylinder. This was not the case for the other two frequencies. The phase advance angle according to Lighthill's analysis is 45 degrees and corresponds to a time advance of 0.0393. This time advance was found to be only about 1/2 of this value and is attained at the 15° and 25° locations, whereas about 2/3 of the value is attained at the 45° location. At 105° the phase advance is near to the predicted value.

Figure 10 presents the streamline flow patterns for various times throughout the fifth cycle for this case. Most outstanding is the pseudo shedding of the vortices that occur. Examination of the patterns show that just prior to the maximum velocity corresponding in time to the point just after the peak drag coefficient, a pseudo shedding of the vortex pair as a unit takes place. The vortex paid starts to reform again between points F and G just prior to where the velocity returns to its mean free-stream value. The vortex pair continues to grow again and reaches a maximum size at the point corresponding to the minimum drag and appears to maintain this length up to the minimum velocity point where again from this point on in time it decreases in size. Point D corresponds to the maximum friction drag coefficient point. Inspection of the flow pattern associated with this point shows

that separation does not occur and so the friction drag should be a maximum. The minimum friction drag coefficient lies between points *I* and *J*. Comparing these flow patterns it is seen that the separation point is at its most forward position. It is of interest to note that at this Reynold's number and frequency, pseudo shedding can be induced.

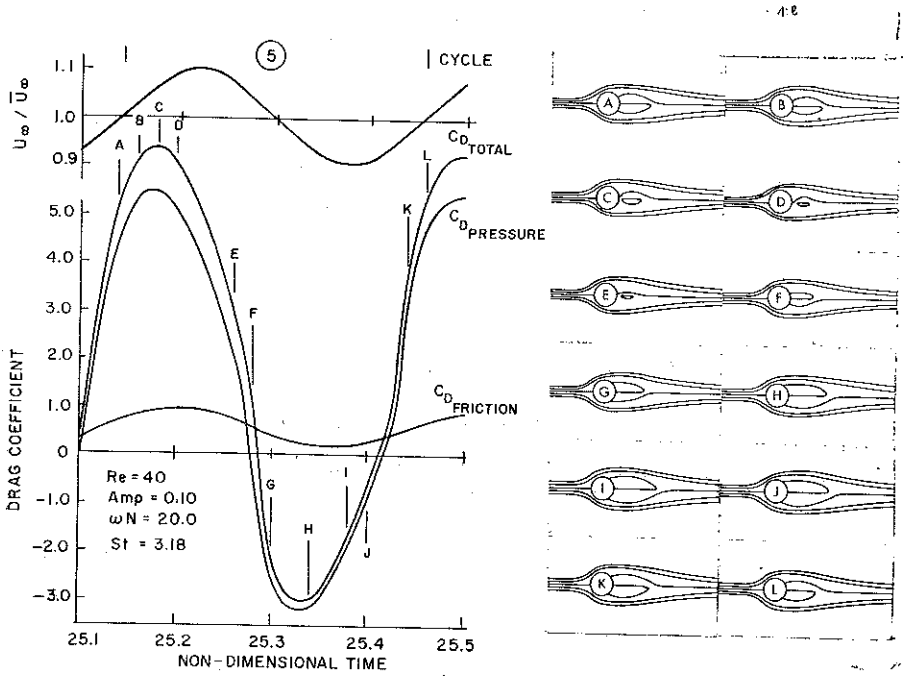

FIG. 10. Flow patterns, fluctuating free-stream Re=40, St=3.18.

b. Reynold's number 200. Numerical solutions for a Reynold's number 200 with a fluctuating free-stream velocity were obtained for a non-dimensional frequency of St=0.149. This frequency corresponds to the natural alternating shedding frequency of the cylinder in a steady free-stream flow.

In Fig. 11 the computed response of the total pressure and friction drag coefficient and total lift coefficient, to free-stream velocity fluctuations are presented. The lift coefficient was considered in addition to the drag, since alternate shedding produces an asymmetrical pressure distribution and so results in a significant amount of lift. The impulsive start was initiated at a non-dimensional time of 63.50 corresponding to a time level after the completion of the limit cycle. Repetitive results start in the second cycle. The effect of the impulsive start is noticeable only during the first 1/2 cycle. Similar to the three cases investigated at Reynold's number 40, the friction drag coefficient follows a very smooth and sinuous curve. The friction drag anticipates the velocity extrema but not however by as great a value as does the pressure of total drag coefficients. In this respect the results obtained for this Reynold's number

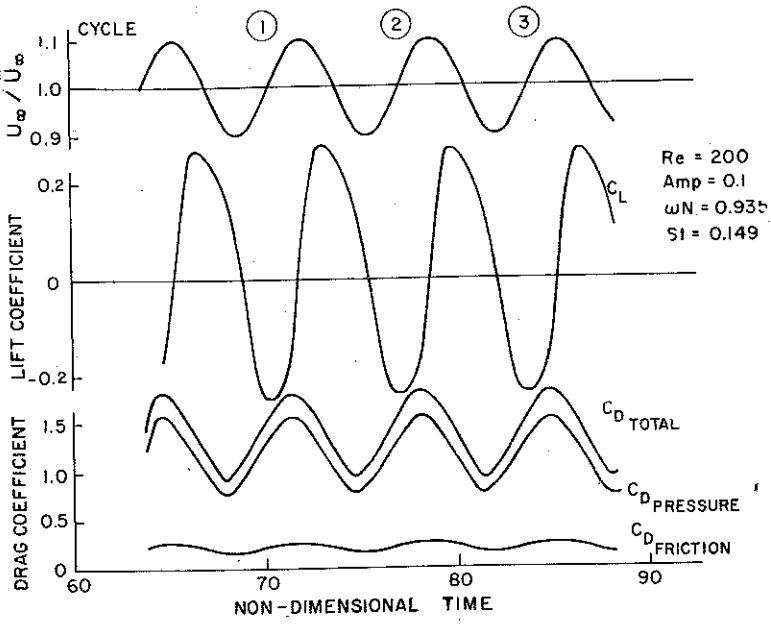

FIG. 11. Drag response to free-stream fluctuations Re=200, St=0.149

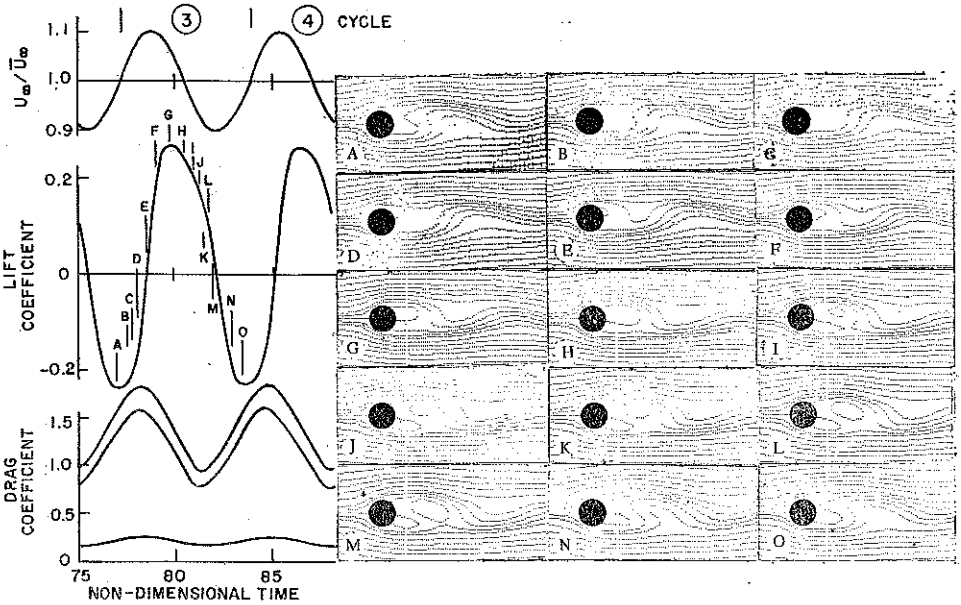

FIG. 12. Flow patterns, fluctuating free-stream Re=200, St=0.149

largely parallel those obtained at a Reynold's number 40. The extrema in lift coefficient lag the extrema in velocity fluctuations. There does not exist as far as is known any results either experimental or analytical that predict the response of the lift coefficient in a fluctuating stream. Thus the results obtained here for the lift may be assumed reasonable only in view of the satisfactory results obtained for the drag. At time 78.0, the flow patterns, Fig. 12, show the start of formation of an attached vortex on the upper rear half. From time 80.5 through the peak at 81.5 the formation of a vortex on the lower rear half and shedding from the upper rear half of the cylinder can be seen.

In Fig. 13 the vorticity response to free-stream velocity fluctuations at Reynolds number 200 and a non-dimensional frequency of 0.149 are shown. According to Lighthill's analysis the phase advance angle is 2 degrees and 40.6 minutes with a corresponding time advance of 0.05. There appears to be a definite lag in the front

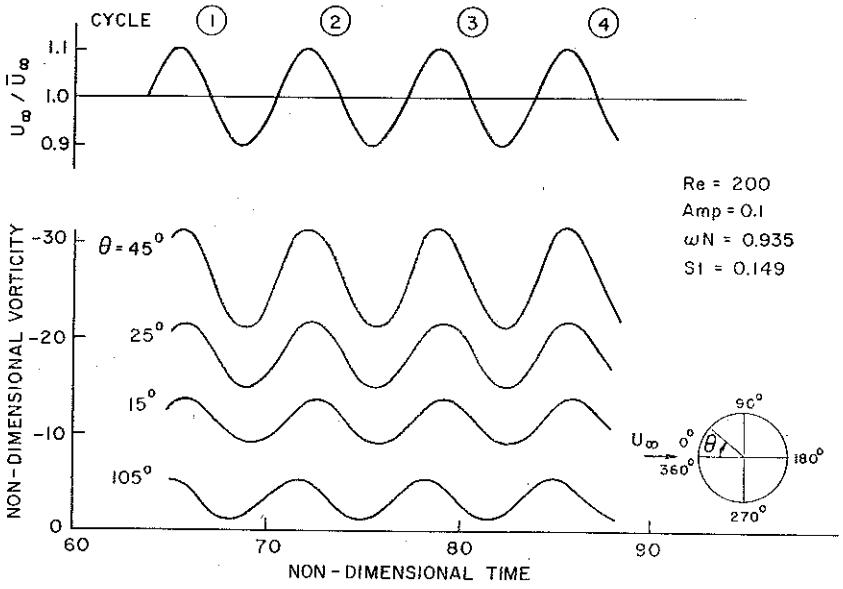

FIG. 13. Vorticity response to free-stream fluctuations Re=200, St=0.149

quadrant as is shown by the curves at 15°, 25°, and 45°. However, at 105° just prior to the fluctuating separation point, the phase advance corresponds to that of the shear flow model. From Fig. 11 it is seen that the time advance of the friction drag coefficient of the cylinder is about 0.50 non-dimensional time units, while for the total drag it is 0.90.

Finally, Fig. 14a shows the relationship between the separation angles φ_1 and φ_2 relative to the oscillations in the free-stream for a Reynold's number 200. Furthermore, a qualitative comparison can be made with the recent results of Tatsuno [16], Fig. 14b, where he investigated the vortex wake behind a circular cylinder oscillating in the flow direction. Tatsuno's results are for Reynold's number 98.8

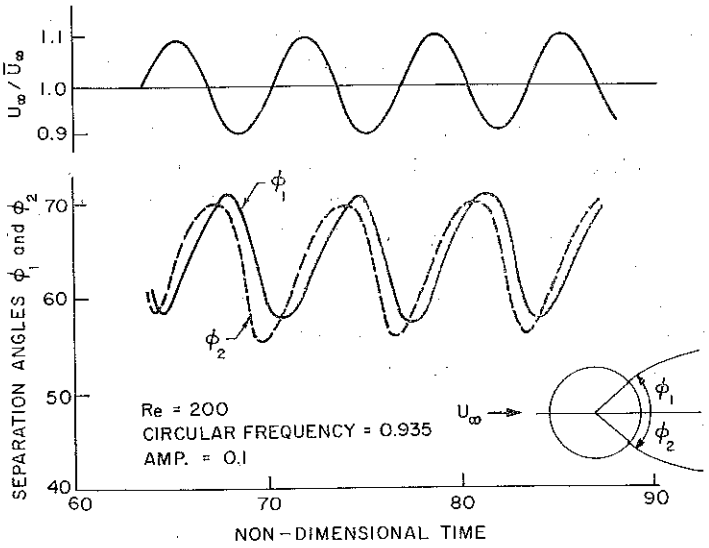

FIG. 14a. Separation point response to free-stream fluactuation Re=200, St=0.149

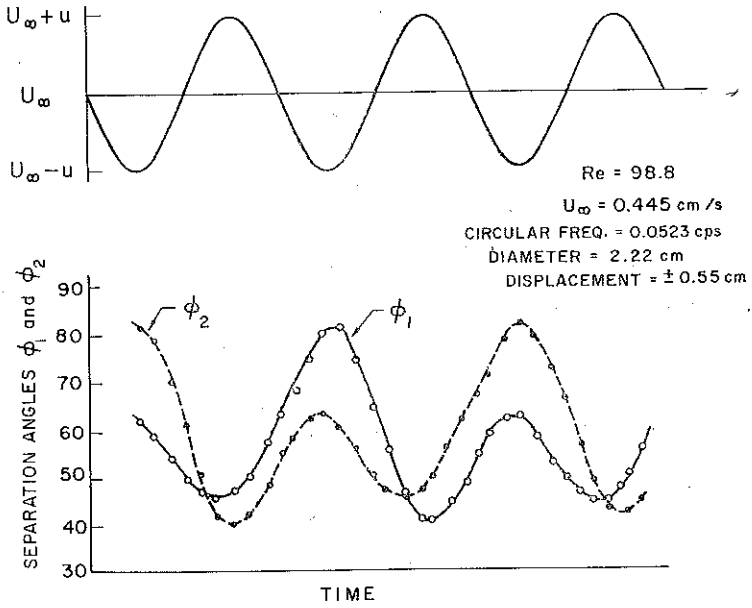

FIG. 14b. Experimental separation point response to free-stream fluctuations Re=98.8 (TATSUNO' 1972)

whereas the present results are for Reynold's number 200, so direct comparison cannot be made, however the numerical results exhibit a similar behavior as the experimental results.

7. Conclusions

a. For the Reynold's number 40 flow in the stagnation point region ($\theta = \pm 45°$), the phase advance or "time of anticipation" was found to be negative for the low and medium frequency cases and positive only for the high frequency. The phase advance for all three frequencies investigated at this Reynold's number, remained essentially constant in the stagnation region, and in this regard the results of this study compare favorably with those of Lighthill.

b. Moving toward the separation point it was found that the "time of anticipation" increases with downstream distance. This was found to be true for all cases investigated. Furthermore, just prior to separation the phase advance is essentially 45° in all cases. This is in excellent agreement with the conjectural reasoning of Lighthill and verifies that his suggested "shear-wave" approximation is valid near separation.

c. Lighthill also surmises that the separation point would fluctuate considerably and with an amplitude that increases with frequency. It was verified by this study that the amplitude of the separation point travel does increase as the frequency increases. It was not feasible in this study to define limits to the extent of this travel.

d. Although not directly comparable with Lighthill's work it is noteworthly that the integrated friction yields a friction drag coefficient that in all cases investigated anticipates the velocity extrema. A positive time of anticipation exists also for the pressure and total drag coefficient.

e. A good description of the movement of the separation angles relative to the free-stream oscillations can be obtained from the present formulation.

References

1. R. E. D. Bishop, and A. Y. Hassan, Proc. Roy. Soc. London, Ser. A, **277**, 1963.
2. C. F. Chen and D. W. Balengee, AIAA, **9**, 2, 1971.
3. S. C. R. Dennis, and Gau-zu Chang, J. Fluid Mech., **42**, 3, 1970.
4. H. G. Dimopulos and T. J. Hanratty, J. Fluid Mech., **33**, 1958.
5. V. P. Goddard, Ph. D. Thesis Univ. of Notre Dame, 1972.
6. A. S. Grove, F. H. Shair, E. E. Petersen and A. Acrivos, J. Fluid Mech., **19**, 1, 1964.
7. I. Hirota and K. Miyakoda, J. Meteor. Soc. Japan, **43**, 1965.
8. M. Kawaguti, Phys. Soc. Japan, **8**, 1953.
9. M. J. Lighthill, Proc. Roy. Soc., London, Ser. A, **224**, 1954.
10. R. B. Payne, J. Fluid Mech., **4**, 1958.
11. E. F. Relf, ARC RM No. 102, 1914.
12. P. J. Roache, *Computational fluid dynamics*, Hermosa Pub., 1972.
13. J. S. Son, Ph. D. Thesis, Dept. Chem. E., Univ. Illinois, 1968.
14. H. Takami, and H. B. Keller, Phys. Fluids Suppl. II, **12**, 1969.

15. S. TANEDA, J. Phys. Soc. Japan, **11**, 1956.
16. M. TATSUNO, Bull. Res. Inst. Appl. Mech., Kyushu Univ., No. 36 1972.
17. D. C. THOMAN, and A. A. SZEWCZYK, Univ. Notre Dame Tech. Rept., No. 66 – 14, 1966.
18. D. C. THOMAN, and A. A. SZEWCZYK, Phys. Fluids Suppl. II, **12**, 1969.
19. D. J. TRITTON, J. Fluid Mech., **6**, 1959.

STRESZCZENIE

NUMERYCZNE ROZWIĄZANIA PROBLEMU LEPKIEGO OPŁYWU WALCA KOŁOWEGO Z UWZGLĘDNIENIEM FLUKTUACJI PRĘDKOŚCI W KIERUNKU STRUMIENIA

Otrzymano rozwiązanie numeryczne dwuwymiarowych, zależnych od czasu równań Naviera-Stokesa, opisujących nieściśliwy opływ walca kołowego z uwzględnieniem fluktuacji prędkości przepływu swobodnego w kierunku ruchu. Fluktuacje przepływu wywołane są jedynie zmianami jego wartości, a nie kierunku. Zależne od czasu równania rozwiązuje się za pomocą schematu różnicowego, posiadającego własności zachowawcze i unoszeniowe w sformułowaniu funkcji prądu i wirowości. Przyjęto zmienny wymiar siatki podziału dla uzyskania takiego wymiaru komórki elementarnej, który byłby zgodny ze strukturą przepływu, a więc siatkę gęstszą założono w obszarach podwyższonych gradientów.

Wyniki przedstawiono dla liczb Reynoldsa od 40 do 200 oraz dla bezwymiarowych częstości strumienia swobodnego w zakresie od 0.02 do 3.2. Wyniki wykazują dobrą zgodność z rozwiązaniami analitycznymi Lighthilla (1954) oraz z danymi doświadczalnymi uzyskanymi przez Chena i Ballengee'go (1971) oraz Tatsuno (1972).

Резюме

ЧИСЛЕННЫЕ РЕШЕНИЯ ПРОБЛЕМЫ ВЯЗКОГО ОБТЕКАНИЯ КРУГОВОГО ЦИЛИНДРА С УЧЕТОМ ФЛУКТУАЦИИ СКОРОСТИ В НАПРАВЛЕНИИ ПОТОКА

Получено численное решение двумерных, зависящих от времени, уравнений Навье-Стокса, описывающих несжимаемое обтекание кругового цилиндра с учетом флуктуаций скорости свободного течения в направлении движения. Флуктуации течения вызваны изменениями только его значения, но не направления. Зависящие от времени уравнения решаются с помощью разностной схемы обладающей свойствами сохрания и переноса в формулировке функции тока и вихрей. Принят переменный размер сетки деления для получения такого размера элементарной ячейки, которая совпадала бы со структурой течения ,т.е. более густую сетку предложено в областях с повышенными градиентами.

Результаты представлены для чисел Рейнольдса от 40 до 200 и для безразмерных частот свободного потока в интервале от 0,02 до 3,2. Результаты показывают хорошее согласие с аналитическими решениями Лайтхилла (1954), а также с экспериментальными данными, полученными Ченом и Балленжом (1971) и Татсуно (1972).

AEROSPACE AND MECHANICAL ENGINEERING
NOTRE DAME, INDIANA

Received September 29, 1973